Fuzzy Skeletonization Improves the Performance of Characterizing Trabecular Bone Micro-architecture

Cheng Chen[1(✉)], Dakai Jin[1], and Punam K. Saha[1,2]

[1] Department of Electrical and Computer Engineering,
University of Iowa, Iowa City, USA
`cheng-chen@uiowa.edu`
[2] Department of Radiology, University of Iowa, Iowa City, USA

Abstract. Skeletonization provides a compact, yet effective representation of an object. Despite limited resolution, most medical imaging applications till date use binary skeletonization which is always associated with thresholding related data loss. A recently-developed fuzzy skeletonization algorithm directly operates on fuzzy objects in the presence of partially volumed voxels and alleviates this data loss. In this paper, the performance of fuzzy skeletonization is examined in a popular biomedical application of characterizing human trabecular bone (TB) plate/rod micro-architecture under limited resolution and compared with a binary method. Experimental results have shown that, using the volumetric topological analysis, fuzzy skeletonization leads to more accurate and reproducible measure of TB plate-width than the binary method. Also, fuzzy skeletonization-based plate-width measure showed a stronger linear association ($R^2 = 0.92$) with the actual bone strength than the binary skeletonization-based measure.

Keywords: Binary and fuzzy skeletonization · Trabecular bone · Volumetric topological analysis

1 Introduction

Skeletonization provides a compact yet effective representation of an object while preserving important topological and geometrical features; see [1,2] for through surveys on applications of skeletonization. Various implementations of skeletonization following the basic principle of Blum's grassfire propagation are available in literature [1,3]. Traditional skeletonization algorithms are defined on binary objects. Recently, Jin and Saha [4] have presented a comprehensive solution for skeletonization of fuzzy object using the theory of fuzzy grassfire propagation and collision impact. However, the influence of fuzzy skeletonization in different applications has not been studied.

Image resolution is a major bottleneck in medical imaging. Often, anatomic structures are acquired in the presence of partial voxel voluming. Despite this

bottleneck, most medical imaging applications [1,2] use the binary skeletoniza-
tion, which is associated with thresholding-induced data-loss and the effects are
magnified at low image resolutions. On the other hand, fuzzy skeletonization may
be directly applied on the fuzzy representation of an object in the presence of
partially volumed voxels without requiring the binarization step. In this paper,
we examine the role of fuzzy skeletonization in measuring trabecular bone (TB)
structure-width or plate-width with limited resolution.

The significance of TB plate/rod distribution in assessing osteoporosis and
low-trauma fracture-risk has long been recognized in histologic studies [5,6],
which have confirmed the relationship between erosion of trabeculae from plates
to rods and higher fracture risk. Various approaches have been reported to dis-
tinguish between rod-like and plate-like trabeculae. The volumetric topological
analysis (VTA) [7] is an effective and powerful method to quantitatively charac-
terize TB plate/rod [8] by computing local TB plate-width based on topological
classification, geodesic distance analysis, and feature propagation on the skeleton
of an object. The performance of VTA is highly dependent on the accuracy of
the skeleton used for plate-width analysis. The original VTA algorithm [7] was
developed for binary objects requiring thresholding on TB images, which is a
sensitive and undesired step at *in vivo* image resolution [9].

The purpose of this work is to determine the influence of fuzzy skeletonization
on the performance of VTA at *in vivo* image resolution, where most bone voxels
are partially volumed. More specifically, we examine the accuracy and repro-
ducibility of plate-widths computed using the fuzzy and binary skeletonization-
based VTA and analyze their abilities to predict the actual bone strength.

2   Methods and Algorithms

In this section, a few definitions and notations and brief outlines of the fuzzy and
binary skeletonization algorithms are presented followed by a short description of
the VTA [7] method used for TB plate-width computation. The *3-D cubic grid*,
denoted as $\mathbb{Z}^3$, where $\mathbb{Z}$ is the set of integers, is used for image representation;
each grid element is referred to as a *voxel*. Conventional definitions of 8- and
4-adjacencies in 2-D and 6-, 18-, and 26-adjacencies in 3-D are followed. This
paper starts with the assumption that the target object is fuzzily segmented
using a suitable segmentation algorithm [10,11]. A *fuzzy object* $\mathcal{O} = (O, f_{\mathcal{O}})$
is a fuzzy set of $\mathbb{Z}^3$, where $f_{\mathcal{O}} : \mathbb{Z}^3 \rightarrow [0,1]$ is the *membership function* and
$O = \{p \in \mathbb{Z}^3 | f_{\mathcal{O}}(p) > 0\}$ is its *support*. In this paper, 26-adjacency is used for
object voxels, i.e., voxels in O, while 6-adjacency is used for background voxels,
i.e., voxels in $\bar{O} = \mathbb{Z}^3 - O$.

2.1   Skeletonization Algorithms

The fuzzy and binary skeletonization algorithms using morphological erosion
under certain topologic and geometric constraints [4,12–15] were chosen for our

comparative study. This simple yet effective approach, outlined in the following, has become popular [1].

Primary Skeletonization

– Locate all *quench* or *skeletal voxel*s in the input object.
– Filter noisy quench voxels and mark *significant skeletal voxel*s.
– Delete unmarked voxels in the increasing order of distance values while preserving the *object topology* and the *continuity of skeletal surfaces*.

Final Skeletonization

– Convert *two-voxel thick* structures into *single-voxel thin* surfaces and curves.
– Remove voxels with *conflicting topologic* and *geometric* properties.

Skeleton Pruning

– Remove *noisy skeletal branches* with low *global significance*.

Binary Skeletization. In binary skeletonization, a fuzzy object $\mathcal{O} = (O, f_{\mathcal{O}})$ is first binarized into $O_{\text{bin}} = \{p | p \in O \wedge f_{\mathcal{O}}(p) > \text{thr}\}$, which is used as input. A constant threshold value of '0.5' is used for 'thr' for all experiments presented in this paper. During primary skeletonization, the centers of maximal balls (CMBs) [16] are located as *binary quench voxel*s using 3-4-5 weighted distance transform (DT) [17,18]. The filtering algorithm by Saha *et al.* [15] is applied to remove noisy quench voxels and select significant surface and curve quench voxels. The four-condition constraint of the (26,6) simple point/voxel characterization by Saha *et al.* [13] is applied for topology preservation. Primary skeletonization produces a "thin set" [19] that has at least one background neighbor except at very busy intersections. During the final skeletonization step, two-voxel thick structures are eroded under topology preservation and some additional geometric constraints [14,15,20] to generate a one-voxel thin skeleton while maintaining its overall shape. Finally, noisy skeletal branches are removed during the pruning step using a *global significance measure* [7].

Fuzzy Skeletization. The fuzzy skeletonization algorithm is directly applied on the fuzzy object $\mathcal{O} = (O, f_{\mathcal{O}})$ without requiring the thresholding step. Here, fuzzy distance transform (FDT) [21] is used instead of binary DT. A *fuzzy quench voxel* [4,22] is located in a fuzzy object by detecting singularity voxels on the FDT map that holds the following inequality for each 26-neighbor q:

$$\text{FDT}(q) - \text{FDT}(p) < \tfrac{1}{2}(f_{\mathcal{O}}(p) + f_{\mathcal{O}}(q))|p - q|, \tag{1}$$

where $|p - q|$ is the Euclidean distance between p, q. During the filtering step in primary skeletonization, the measure of *collision impact* ξ_{D} [4] is used to define the local significance of individual fuzzy quench voxels.

$$\xi_{\text{D}}(p) = 1 - \max_{q \in N_{26}^*(p)} \frac{f_+(\text{FDT}(q) - \text{FDT}(p))}{\tfrac{1}{2}(f_{\mathcal{O}}(p) + f_{\mathcal{O}}(q))|p - q|}. \tag{2}$$

Collision impact at a quench voxel relates to the angle where independent fire-fronts collide. The value is high when fire-fronts make a head-on collision. Quench voxels on a core skeletal structure have high values of collision impact, while those on a skeletal branch emanating from a noisy protrusion have low values [4]. Jin and Saha [4] locally characterized the surface- and curve-like fuzzy quench voxels and argued the use of different filtering kernels for them.

For topology preservation, the constraints of 3-D simple pints/voxels [13] are applied on the support of the fuzzy object. Moreover, it is possible to find examples in fuzzy skeletonization, where the criteria of quench voxels and 3-D simple voxels fail to maintain the continuity of skeletal surfaces. Thus, to ensure the continuity of skeletal surfaces, additional constraints of (8,4) 2-D simple points are applied on each of the three coordinate planes through the candidate voxel [4]. Similar to binary skeletonization, two-voxel thick structures are converted into a single-voxel thin skeleton during final skeletonization. A few thick-voxels survive the first step of final skeletonization, which are eliminated using the conflict between their topologic and geometric properties. Finally, a collision impact-weighted path length of individual skeletal branches is used as their global significance during the pruning step [4].

Volumetric Topological Analysis. VTA calculates the plate-width of individual trabeculae in the unit of microns and uses this measure to locally classify individual trabecular type on the continuum between a perfect plate (green) and a perfect rod (red) (Fig. 1a). Note that the VTA-measured plate-width (Fig. 1b) is different from either thickness or skeleton-width. Figure 2 presents the results of intermediate steps of VTA. First, a surface representation of an object is computed using a suitable skeletonization algorithm [3]. Different topological entities, including surface-interior, surface-edge, curve, and junction voxels, are identified on the surface skeleton using digital topological analysis [23] (Fig. 2b). The geodesic distance transform (GDT) (Fig. 2c) is applied on the surface skeleton, which computes the geodesic distance of individual skeletal voxels from the edge; GDT at surface-edge as well as curve voxels are initialized as their FDT values, which enables the computation of plate-width instead of skeleton-width (see Fig. 1b). Using this convention for initialization, the GDT value at an axial voxel, i.e., a voxel on the arc skeleton, gives the value of half plate-width. However, the same is not true at non-arc skeletal voxels, where the plate-width measure is derived from the nearest arc skeletal voxel using a feature-propagation algorithm [24] (Fig. 2d). Finally, another level of feature propagation is applied to propagate plate-width measures from the surface-skeleton to the entire object volume, i.e., from Fig. 2d to 2e. Both feature propagation steps are performed using the principle established by Liu et al. [24] that is independent of scan or processing order. See [7] for detail and accurate description of different steps.

Let $\mathcal{O}_{\mathrm{BVF}} = (O_{\mathrm{BVF}}, f_{\mathrm{BVF}})$ denote the bone volume fraction (BVF) image of TB, where O_{BVF} is the support with non-zero BVF. The method presented in [24] was used to compute the BVF map in a CT image. Let $\mathrm{VTA}_{\mathrm{FSK}}(p)$ denote the TB plate-width at p using fuzzy skeletonization based VTA algorithm.
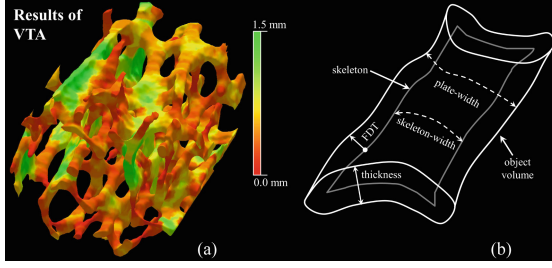
Fig. 1. (a) Trabecular bone plate/rod classification using volumetric topological analysis (VTA). (b) Various measures on a schematic drawing of a plate-like structure (color figure online).

The fuzzy skeletonization-based average plate-width (PW_{FSK}) characterizing the overall plate/rod micro-architecture of $\mathcal{O}_{BVF}$ is defined as follows:

$$PW_{FSK} = \frac{\sum_{p \in O_{BVF}} VTA_{FSK}(p) f_{BVF}(p)}{\sum_{p \in O_{BVF}} f_{BVF}(p)} \tag{3}$$

The average plate-width measure PW_{BSK} using binary skeletonization was similarly computed using $VTA_{BSK}(p)$.

3 Experiments and Results

Results of surface skeleton and local plate-width computation from VTA are presented in Fig. 3. In general, binary skeletonization over erodes TB surfaces, which makes the computed plate-width lower than true plate-width and results in more rod-like (reddish) trabeculae. Also, binary skeletonization created a few noisy branches (indicated by red arrows) and less-smooth skeletal surfaces (indicated by blue arrows). On the other hand, fuzzy skeletonization generated smoother surfaces and yielded expected measures of plate-width.

Three quantitative experiments were designed to evaluate the following — (1) accuracy, (2) repeat scan reproducibility, and (3) ability to predict bone strength. Computer-generated phantoms were used for Experiment 1. Multi-row detector CT (MD-CT) imaging of cadaveric TB specimens were used for Experiments 2 and 3. For Experiment 3, bone strength of cadaveric specimens was determined by mechanical testing.

3.1 Experimental Methods

Computer-Generated Phantoms. Computerized phantoms with known plate-widths were generated to examine the accuracy of fuzzy and binary skeletonization-based VTA algorithms. First, 3-D binary objects with boundary-noise and their true skeletons were generated at a high resolution over an array
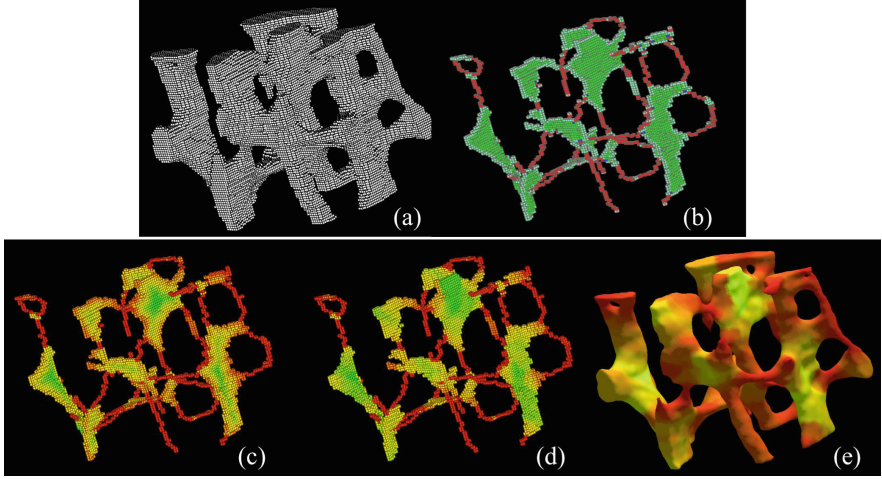
Fig. 2. Intermediate steps of the VTA algorithm. (a) A region from a micro-CT image of a TB specimen. (b) Classified topological entities including surface (green), curves (red), edges (light), and junctions (blue) on the surface skeleton. (c-e) Color coded display of geodesic distance transform (c), plate-width (d) and surface rendition of VTA over the bone volume (e) (color figure online).

of $512 \times 512 \times 512$. Test phantoms were generated from binary objects by down-sampling. The process starts by sampling ideal sinusoids of known skeleton-width, say w_S; let S denote the set of sampled points. A 3-D object V was computed from S by computing a distance transform from S, thresholding it at a value, say w_d, and, finally, adding random noisy protrusion of three-voxel diameter on the object boundary. The plate-width of the binary object V was recorded as $w_V = w_S + 2 \times w_d$. The test phantom V_{test} was generated by down-sampling V using a $3 \times 3 \times 3$ window to simulate fuzziness. Ten test phantoms were generated with their plate-width $w_V = 3, 5, \cdots, 21$ in the voxel unit of the down-sampled image. For fuzzy skeletonization-based VTA, the test phantom V_{test} was directly used as the input. For binary skeletonization, a threshold of 0.5 was applied on V_{test}.

Cadaveric Specimens and MD-CT Imaging. Fifteen fresh-frozen human cadaveric ankle specimens were obtained from 11 body donors (age: 55 to 91 years) under the Deeded Bodies Program, The University of Iowa. The ankle specimens were removed at the mid-tibia region. Exclusion criteria for this study were evidence of previous fracture or knowledge of bone tumor or bone metasta-sis. These specimens were kept frozen until the performance of MD-CT imaging. High resolution MD-CT scans of the distal tibia were acquired on a 128-slice SOMATOM Definition Flash scanner (Siemens, Munich, Germany) using the following CT parameters: single tube spiral acquisition at 120 kV, 200 effective mAs, 1 sec rotation speed, pitch factor: 1.0, nominal collimation: 16×0.3 mm, scan length: 10 cm beginning at the distal tibia end-plateau, and total effective
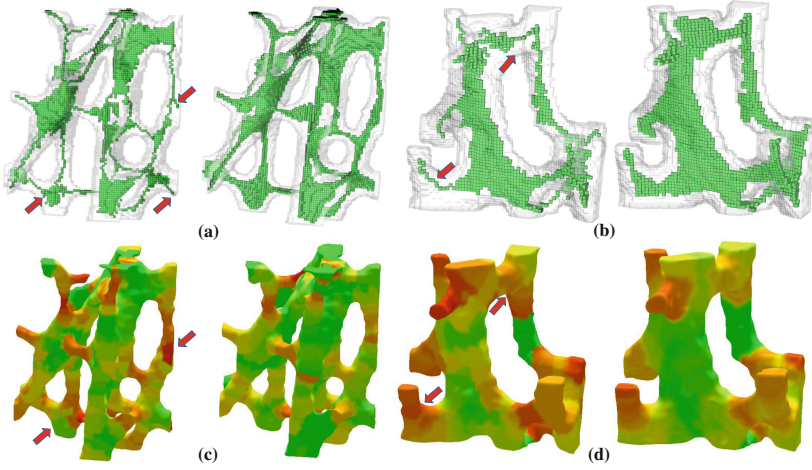
Fig. 3. Results of binary and fuzzy skeletonization on two small regions from TB images are shown in (a) and (b), respectively. Results of local plate-width on the same image regions using binary and fuzzy skeletonization-based VTA are shown in (c) and (d) respectively. The same color coding bar of Fig. 1 are used here (color figure online).

dose equivalent to 17 mrem $\approx$ 20 days of environmental radiation in the USA. Images were reconstructed at 0.2 *mm* slice thickness and 0.2×0.2 in-plane resolution using a special U70u kernel achieving high structural resolution. Three MD-CT repeat scans were acquired for each specimen with repositioning the phantom between scans.

Mechanical Testing for Bone Strength. To determine TB strength, a cylindrical TB core 8 *mm* in diameter and 20.9±3.3 *mm* in length was cored from the distal tibia *in situ* along the proximal-distal direction. Each TB core was mechanically tested for compression using an electromechanical materials testing machine. To minimize specimen end effects, strain was measured with a 6 *mm* gauge length extensometer attached directly to the midsection of the bone. A compressive preload of 10 N was applied and strains were set to zero. At a strain rate of 0.005 sec^{-1}, each specimen was preconditioned to a low strain with at least ten cycles and then loaded to failure. Yield stress was determined as the intersection of the stress-strain curve and a 0.2 % strain offset of the modulus.

3.2   Results and Discussion

Accuracy. To examine the accuracy of computed plate-width, an error was defined as the mean absolute difference between computed and true plate-widths; let Error$_{\mathrm{FSK}}$ and Error$_{\mathrm{BSK}}$ denote errors of fuzzy and binary skeletonization-based plate-width computation. The mean and standard deviation of Error$_{\mathrm{BSK}}$ over ten test phantoms were 1.50±0.15 in the down-sampled voxel unit. The

observed mean and standard deviation of $Error_{FSK}$ was 0.40 ± 0.02, a 73 % reduction compared to $Error_{BSK}$. A paired t-test result ($p < 0.001$) confirmed the significance of the error reduction. Also, it is encouraging to note that the mean error of $Error_{FSK}$ is around 0.4 voxel unit, while the digital localization error in skeletonization is 0.38 [25]. Thus, it may be inferred that the primary source of error in $Error_{BSK}$ is digital localization.

Reproducibility. Two different analyses were performed using the three repeat-scan MD-CT images of fifteen cadaveric TB specimens to examine the reproducibility. First, the mean absolute mutual difference (MAMD) of PW_{FSK} (or PW_{BSK}) was computed over matching regions in post-registered repeat MD-CT scans of each TB specimen. The results of MAMD analysis are presented in Fig. 4(a). It is observed that MAMD of PW_{FSK} is consistently lower than that of PW_{BSK} for each TB specimen and a paired t-test confirmed that the reduction in MAMD using fuzzy skeletonization is statistically significant ($p < 0.001$)
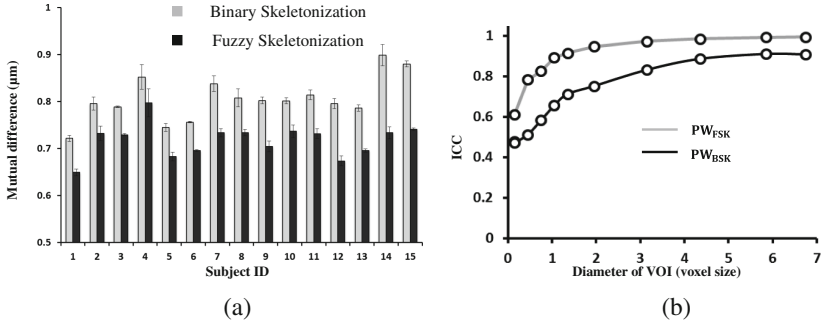

Fig. 4. (a) Mutual difference between fuzzy skeletons and binary skeletons of three repeat-scan CT images of fifteen cadaveric trabecular bone specimens. (b) Reproducibility of plate-width computed from binary and fuzzy skeleton in three repeat scans of CT images.

The intraclass correlation (ICC) of PW_{FSK} (or PW_{BSK}) was computed over matching spherical volume of interests (VOIs) in post-registered TB repeat MD-CT scans. Ten spherical VOIs were randomly selected in the first scan of each TB specimen (a total of 150 VOIs). Each VOI was located at least 8 mm proximal to the distal endplate. A post-registration algorithm was used to locate the matching VOIs in the second and third repeat scans. The VOI size was varied, and the ICC values were presented in Fig. 4(b) as a function of VOI diameter. The fuzzy skeletonization-based measure PW_{FSK} achieves an ICC of 0.95 at a VOI diameter of 1.05 mm or greater and it converges to the value of 0.98. In contrast, the binary skeletonization-based measure PW_{BSK} achieves the highest ICC value of 0.91 over the range of VOI diameters of our experiment.

Ability to Predict Bone Strength. Results of correlation analysis between TB yield stress and the average plate-width computed from binary and fuzzy
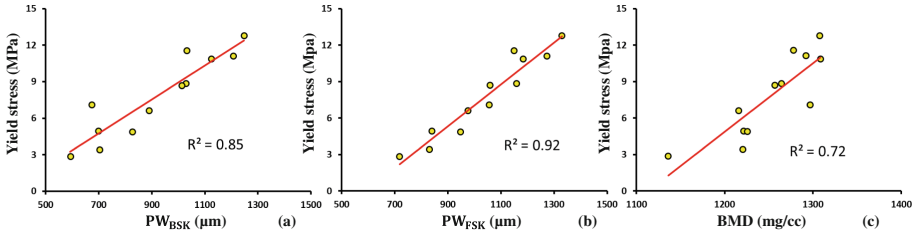
Fig. 5. Ability of different TB measures to predict experimental bone strength: (a) PW_{BSK} (b) PW_{FSK} (c) BMD. The ability is computed in terms of the R^2 of linear correlation between bone strength and respective measures.

skeletonization are presented in Fig. 5. PW_{FSK} achieves the value of 0.92 for R^2 or the coefficient of determination from linear regression analysis. On the other hand, R^2 of PW_{BSK} was 0.85. Note that both measures achieves higher linear correlation with yield stress as compared to the simple measure of average bone mineral density (BMD), in which the R^2 was 0.74. This observed results reaffirm the importance of TB plate/rod mirco-architecture as well as the superiority of fuzzy skeletonization over the binary method in capturing TB micro-structural properties at *in vivo* resolution.

4   Conclusion

This paper has evaluated the role of fuzzy skeletonization in characterizing TB micro-architecture at *in vivo* image resolution. The experimental results have demonstrated that fuzzy skeletonization effectively eliminates the binarization step which is always associated with data loss, especially, at regions with limited resolution. It is experimentally confirmed that fuzzy skeletonization-based TB plate-width is significantly more accurate and reproducible as compared to the binary skeletonization-based measure. Further, it was found in a cadaveric study that the fuzzy skeletonization-based TB plate-width measure has a stronger association with actual bone strength than the binary method. In the context of the specific application, the quality of surface skeleton influences the performance of volumetric topological analysis (VTA) where surface skeleton heavily determines the accuracy of plate-width. The improvement of plate-width using fuzzy skeletonization also indicates that fuzzy skeletonization generates more accurate skeleton than the binary method, possibly, by removing over erosion and false branches.

References

1. Saha, P.K., Borgefors, G., di Baja, G.S.: A survey on skeletonization algorithms and their applications. Pattern Recogn. Lett. (2015). http://www.sciencedirect.com/science/article/pii/S0167865515001233

2. Saha, P., Strand, R., Borgefors, G.: Digital topology and geometry in medical imaging: a survey. IEEE Trans. Med. Imag. **34**(9), 1940–1964 (2015)

3. Siddiqi, K., Pizer, S.M.: Medial Representations: Mathematics, Algorithms and Applications, vol. 37. Springer, The Netherlands (2008)

4. Jin, D., Saha, P.K.: A new fuzzy skeletonization algorithm and its applications to medical imaging. In: Petrosino, A. (ed.) ICIAP 2013, Part I. LNCS, vol. 8156, pp. 662–671. Springer, Heidelberg (2013)

5. Kleerekoper, M., Villanueva, A.R., Stanciu, J., Rao, D.S., Parfitt, A.M.: The role of three-dimensional trabecular microstructure in the pathogenesis of vertebral compression fractures. Calc. Tiss. Int. **37**, 594–597 (1985)

6. Recker, R.R.: Architecture and vertebral fracture. Calc. Tiss. Int. **53**(Suppl 1), S139–142 (1993)

7. Saha, P.K., Xu, Y., Duan, H., Heiner, A., Liang, G.: Volumetric topological analysis: a novel approach for trabecular bone classification on the continuum between plates and rods. IEEE Trans. Med. Imag. **29**(11), 1821–1838 (2010)

8. Chen, C., Jin, D., Liu, Y., Wehrli, F.W., Chang, G., Snyder, P.J., Regatte, R.R., Saha, P.K.: Volumetric topological analysis on in vivo trabecular bone magnetic resonance imaging. In: Bebis, G., Boyle, R., Parvin, B., Koracin, D., McMahan, R., Jerald, J., Zhang, H., Drucker, S.M., Kambhamettu, C., Choubassi, M., Deng, Z., Carlson, M. (eds.) ISVC 2014, Part I. LNCS, vol. 8887, pp. 501–510. Springer, Heidelberg (2014)

9. Krug, R., Burghardt, A.J., Majumdar, S., Link, T.M.: High-resolution imaging techniques for the assessment of osteoporosis. Radiol. Clin. North Am. **48**(3), 601–621 (2010)

10. Saha, P.K., Udupa, J.K., Odhner, D.: Scale-based fuzzy connected image segmentation: theory, algorithms, and validation. Comp. Vis. Imag. Und. **77**, 145–174 (2000)

11. Sonka, M., Hlavac, V., Boyle, R.: Image Processing, Analysis, and Machine Vision, 3rd edn. Thomson Engineering, Toronto, Canada (2007)

12. Jin, D., Iyer, K.S., Chen, C., Hoffman, E.A., Saha, P.K.: A robust and efficient curve skeletonization algorithm for tree-like objects using minimum cost paths. Pattern Recogn. Lett. (2015). http://www.sciencedirect.com/science/article/pii/S0167865515001063

13. Saha, P.K., Chaudhuri, B.B.: Detection of 3-D simple points for topology preserving transformations with application to thinning. IEEE Trans. Patt. Anal. Mach. Intell. **16**, 1028–1032 (1994)

14. Sanniti di Baja, G.: Well-shaped, stable, and reversible skeletons from the (3,4)-distance transform. J. Vis. Commun. Image Represent. **5**, 107–115 (1994)

15. Saha, P.K., Chaudhuri, B.B., Majumder, D.D.: A new shape preserving parallel thinning algorithm for 3D digital images. Pat. Recog. **30**, 1939–1955 (1997)

16. Arcelli, C., Sanniti di Baja, G.: Finding local maxima in a pseudo- euclidean distance transform. Comp. Vis. Graph Imag. Proc. **43**, 361–367 (1988)

17. Borgefors, G.: Distance transformations in digital images. Comp. Vis. Graph Imag. Proc. **34**, 344–371 (1986)

18. Borgefors, G.: Distance transform in arbitrary dimensions. Comp. Vis. Graph Imag. Proc. **27**, 321–345 (1984)

19. Arcelli, C., Sanniti di Baja, G.: A width-independent fast thinning algorithm. IEEE Trans. Patt. Anal. Mach. Intell. **7**(4), 463–474 (1985)

20. Arcelli, C., Sanniti di Baja, G., Serino, L.: Distance-driven skeletonization in voxel images. IEEE Trans. Patt. Anal. Mach. Intell. **33**(4), 709–720 (2011)

21. Saha, P.K., Wehrli, F.W., Gomberg, B.R.: Fuzzy distance transform: theory, algorithms, and applications. Comp. Vis. Imag. Und. **86**, 171–190 (2002)
22. Svensson, S.: Aspects on the reverse fuzzy distance transform. Pat. Recog. Lett. **29**, 888–896 (2008)
23. Saha, P.K., Chaudhuri, B.B.: 3D digital topology under binary transformation with applications. Comp. Vis. Imag. Und. **63**, 418–429 (1996)
24. Liu, Y., Jin, D., Li, C., Janz, K.F., Burns, T.L., Torner, J.C., Levy, S.M., Saha, P.K.: A robust algorithm for thickness computation at low resolution and its application to in vivo trabecular bone CT imaging. IEEE Trans. Biomed. Eng. **61**(7), 2057–2069 (2014)
25. Saha, P.K., Wehrli, F.W.: Measurement of trabecular bone thickness in the limited resolution regime of in vivo MRI by fuzzy distance transform. IEEE Trans. Med. Imag. **23**, 53–62 (2004)